Water evaporation model of a catalyst converter in the context of hybrid electric vehicles energy and pollutants management

Jean Kuchly, Maxime Doussot, Antoine Simon, Thierry Jaine, Dominique Nelson-Gruel, Alain Charlet, Cédric Nouillant, Yann Chamaillard

Water evaporation model of a catalyst converter in the context of hybrid electric vehicles energy and pollutants management

Jean Kuchly*,**, Maxime Doussot*,***, Antoine Simon*, Thierry Jaine*, Dominique Nelson-Gruel**, Alain Charlet**, Cédric Nouillant*, Yann Chamaillard**

*Stellantis, 212 boulevard Pelletier 78955 Carrières-sous-Poissy, France (e-mail: jean.kuchly@stellantis.com)
**Laboratoire PRISME, 8 rue Léonard de Vinci 45100 Orléans, France
***IFP Energie nouvelles, 1-4 Av de Bois Préau 92852 Rueil-Malmaison, France

Abstract: The energy and pollutants management of Hybrid Electric Vehicles (HEV) consists in determining at each instant the optimal torque split between the Internal Combustion Engine (ICE) and the Electric Motor (EM). This torque choice aims to minimize both fuel consumption and pollutants emissions. A critical piece of information in this context is the value of the Three-Way Catalyst Converter (3WCC) conversion efficiency. This value is highly dependent on the 3WCC temperature; it is hence of major importance to have an accurate estimation of it. Although the literature is abundant about simple 0D thermal models of 3WCC, it is tempting to implement a more accurate and consequently complex model. In particular, both moisture from the exhaust gases during engine start and from ambient air during cooling phases lead to the formation of a liquid water film on the monolith's exchange surface, causing a strong temperature plateau during the warm-up phase. The water evaporation causing a delay in the 3WCC temperature increase, it could lead to a serious degradation of the pollutants emissions if not taken into account. This paper proposes hence a 1D thermal model including water phase changing that allows a 72% decrease in the 3WCC temperature estimation error during the warm up phase. This accuracy gain, occurring in a phase where the converter temperature has not reached its full efficiency, provides a 1-2% reduction in CO, HC and NOx emissions.

Keywords: Optimal control, HEV energy management, 3WCC converter, thermal modelling, pollutants

1. INTRODUCTION

Two critical problems related to the combustion of fuels are air pollution and global warming. In this context, regulatory standards have emerged to limit the environmental impact of many industrial sectors. Automotive manufacturers in particular have to face challenging regulations that led to remarkable changes in the powertrain domain. Among solutions chosen by the manufacturers, HEVs are a promising way to decrease the carbon footprint of transport and the atmospheric pollution in densely populated areas.

In this paper, a parallel hybrid architecture is considered (Fig. 1). In this architecture, the torques produced by the ICE (τ_{CR}) and by the EM (τ_{EM}) add directly to satisfy the torque request of the driver (τ_{CR}), expressed at the crankshaft:

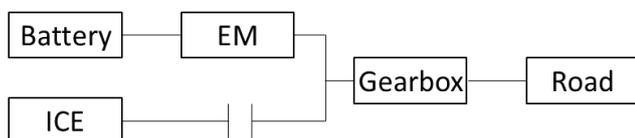$$\tau_{CR} = \tau_{ICE} + \tau_{EM} \qquad (1)$$

Fig. 1 Parallel hybrid architecture

The possibility to modify the functionning points of both ICE and EM by manipulating the torque split in (1) allows to benefit from the advantages of both devices. In most of the literature, this degree of freedom is used to minimize fuel consumption only by moving ICE functionning points towards fuel efficient zones (Hadj-Said, 2016; Nüesch, 2014; Di Cairano, 2013). However, as illustrated in the specific fuel consumption and NOx maps displayed in Fig. 2 and Fig. 3, the best zone for fuel consumption may also be the worst for pollutants generation. Fuel consumption and pollutants emissions are therefore antagonist objectives and have to be minimized conjointly (Michel, 2012; Simon, 2018; Kuchly, 2020); other objectives can also be taken into account, such as noise reduction (Aliramezani, 2018) and battery aging (Sciaretta, 2014). The energy and pollutants management can be defined as the optimal control problem aiming to compute the torque split in order to minimize the following criterion:

$$J = \int_0^{tf} \left(\dot{m}_{fuel}(t) + \alpha\, \dot{m}_{poll}(t) \right) dt, \qquad (2)$$

where $\dot{m}_{fuel}$ is the fuel consumption and $\dot{m}_{poll}$ the pollutants terms is typically a weighted sum of the regulated pollutants mass flows. Hence, considering carbon monoxide (CO), unburnt hydrocarbons (HC) and nitrogen oxides (NOx):

$$
\begin{aligned}
\dot{m}_{poll}(t) &= \beta\, \eta_{CO}(t)\dot{m}_{CO}(t) + \gamma\, \eta_{HC}(t)\dot{m}_{HC}(t) \\
&\quad + \kappa\, \eta_{NO_x}(t)\dot{m}_{NO_x}(t),
\end{aligned}
\qquad (3)
$$

where $\dot{m}_{CO}$, $\dot{m}_{HC}$, and $\dot{m}_{NO_x}$ are respectively the generation by the ICE of CO, HC and NO_x,; η_{CO}, η_{HC}, and η_{NO_x} are the corresponding conversion efficiencies of the 3WCC and β, γ and κ are the weighting factors chosen by the designer.
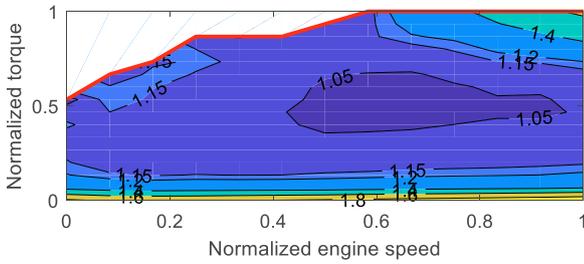

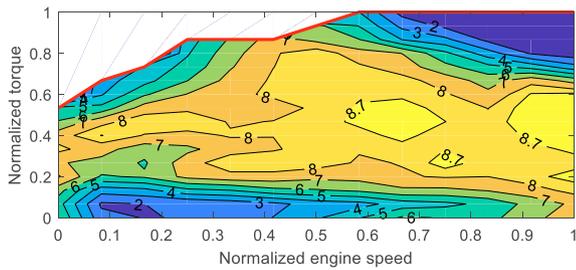Fig.2: Normalized specific fuel consumption map

Fig.3: Normalized specific NO_x generation

The conversion efficiency is merely dependant on gas flow, known usually from a map from experimental data, and on the 3WCC temperature. It is then of critical importance for the energy and pollutants management system to base its decisions on reliable information concerning the 3WCC temperature. Introducing a thermocouple directly in the 3WCC monolith would damage it, beyond the industrial costs and the failure risk. Solutions proposed in the literature to overcome this problem rely either on a thermal model in open-loop (Maamria, 2017; Michel, 2015) or on an Extended Kalman Filter (EKF) that includes also a thermal model (Simon, 2019; Utz, 2014). If a vast majority of authors have chosen a simple, 0D thermal model (Michel, 2017; Maamria, 2014; Simon, 2015), a 1D model able to represent the temperature gradient in the 3WCC could improve the accuracy of the estimation (Simon, 2018). Moreover, as illustrated in Fig. 4, the evaporation of the water initially present in the 3WCC has a major impact on temperature during warm-up.

Regarding the antagonism between the necessity of an accurate temperature estimation and the computational constraints resulting from the embedded context of the automotive industry, a legitimate problematic is to determine the influence of model improvement on pollutants performances. This paper aims to answer this question. In section II a 1D model including water phase changing and a classical 0D model are proposed and described. In section III the optimal control strategy used to test the two models is detailed. In section IV the pollutants emissions performances of strategies considering each model are compared in the context of energy and pollutants management of HEVs.
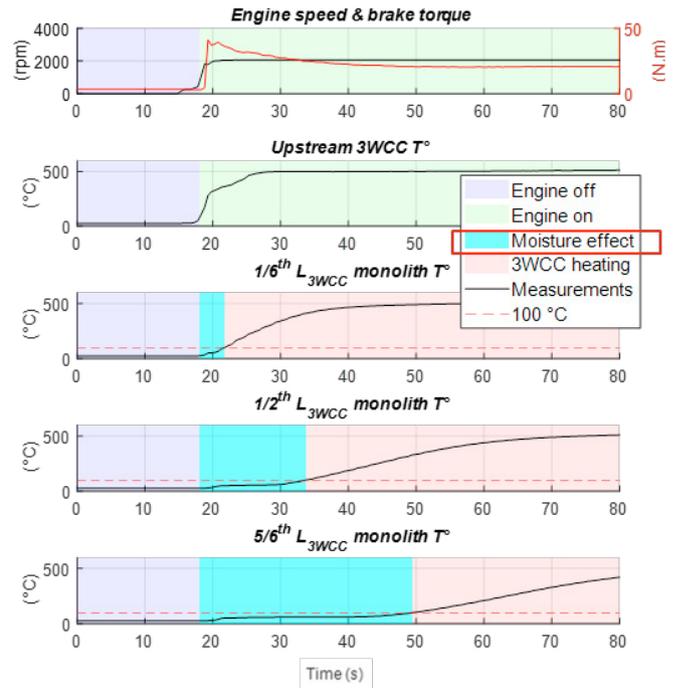
Fig. 4: Impact of moisture on 3WCC temperature

2. 1D MODEL INCLUDING WATER PHASE CHANGING

2.1 1D Model

For clarity purpose, all variables and constants used in this paper are listed in Appendix A, Table 2. The 1D model proposed in this paper considers a spatial discretisation of the 3WCC into 3 nodes along its longitudinal axis (Fig. 5).
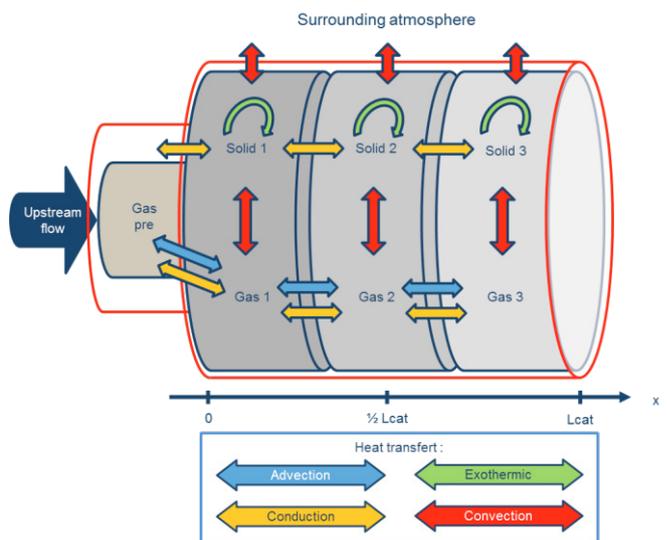
Fig. 5: Spatial discretisation of the 3WCC

The considered states are then, for each node, the 3WCC monolith temperature, the exhaust gas temperature, the water fraction in exhaust gas and the condensed water mass. At each

time iteration of the model, the following procedure is followed:

1) The exhaust gas flow, pressure and temperature upstream of the 3WCC (respectively $\dot{m}_{exh}$, P_{exh} and $T_{exh,up}$) and the pollutants flows $\dot{m}_{CO}$, $\dot{m}_{HC}$, and $\dot{m}_{NO_x}$ are obtained from maps of engine speed and torque.

2) The exhaust gas properties are determined. The density is obtained from the ideal gas law. The heat capacity, the dynamic viscosity and the thermal conductivity are obtained from empirical formulas (Chase, 1998). Finally, the cinematic viscosity is obtained from the dynamic viscosity and the density.

$$\rho_{exh}(t,x) = \frac{P_{exh}(t)}{r_{exh}T_{exh}(t,x)} \tag{4}$$

$$cp_{exh}(t,x) = 0.2982 \,.\, T_{exh}(t,x) + 974.3402 \tag{5}$$

$$\begin{aligned}\mu_{exh}(t,x) \\ = 8.88\,.\,10^{-15}\,.\,T_{exh}^3(t,x) - 3.24\,.\,10^{-11}\,.\,T_{exh}^2(t,x) \\ + 6.27\,.\,10^{-8}\,.\,T_{exh}(t,x) + 2.35\,.\,10^{-6}\end{aligned} \tag{6}$$

$$\begin{aligned}\lambda_{exh}(t,x) \\ = 1.52\,.\,10^{-11}\,.\,T_{exh}^3(t,x) - 4.86\,.\,10^{-8}\,.\,T_{exh}^2(t,x) \\ + 1.02\,.\,10^{-4}\,T_{exh}(t,x) + 3.93\,.\,10^{-4}\end{aligned} \tag{7}$$

$$\nu_{exh}(t) = \mu_{exh}(t)\rho_{exh}(t) \tag{8}$$

3) Reynolds, Prandtl and Nusselt numbers are computed in order to obtain the internal convection coefficient. Since it appears according to the Reynolds number that the flow is laminar for all functioning points, the Sieder-Tate correlation for laminar flows is chosen in (13). The exhaust gas viscosity at the convection surface temperature $\mu_{exh\,s}$ is approximated equal to μ_{exh}, leading to simplify the ratio $\left(\frac{\mu_{exh}}{\mu_{exh\,s}}\right)^{0.14}$ as equal to 1.

$$Re(t,x) = \frac{\rho_{exh}(t,x)\,u_{exh}(t,x)\,L}{\mu_{exh}(t,x)} \tag{9}$$

$$u_{exh}(t,x) = \frac{\dot{m}_{exh}(t)}{\rho_{exh}(t,x)A_{cs}} \tag{10}$$

$$Pr(t,x) = \frac{cp_{exh}(t,x)\mu_{exh}(t,x)}{\lambda_{exh}(t,x)} \tag{11}$$

$$Nu(t,x) = 1.86\,(Re(t,x)Pr(t,x))^{0.33}\,.\left(\frac{\phi_{canal}}{L}\right)^{0.33} \tag{12}$$

$$h_{in}(t,x) = \frac{L}{\lambda_{exh}(t,x)\,.\,Nu(t,x)} \tag{13}$$

4) The liquid water mass dynamic is led by two factors: the water vapour fraction difference between the exhaust gas and the liquid/gas boundary, and the thermal difference between the condensed water and the exhaust gas. In order to simplify the model, the temperature of the condensed water is approximated equal to the 3WCC temperature. The dynamic of the water vapour fraction $Y_{H_2O,exh}$ and the

condensed water mass m_{H_2O} are derived from (Clarkson, 1995; Furfaro, 2015):

$$\begin{aligned}\frac{\partial Y_{H_2O,exh}(t,x)}{\partial t} \\ = \frac{\dot{m}_{H_2O}(t,x)}{\rho_{exh}(t,x)V_{exh}} + \frac{D_{H_2O\,vap}}{\rho_{exh}(t,x)}\,.\,\frac{\partial^2 Y_{H_2O,exh}(t,x)}{\partial x^2} \\ - u_{exh}(t,x)\frac{\partial Y_{H_2O,exh(t,x)}}{\partial x}\end{aligned} \tag{14}$$

$$V_{exh} = V_{cat}\cdot\epsilon\cdot\frac{dx}{L} \tag{15}$$

$$\dot{m}_{H_2O}(t,x) = \dot{m}_{H_2O,diff}(t,x) + \dot{m}_{H_2O,th}(t,x) \tag{16}$$

$$\begin{aligned}\dot{m}_{H_2O,diff}(t,x) \\ = \rho_{exh}(t,x)K_{H_2O}A_{in} \\ \cdot\left(Y_{H_2O,exh}(t,x) - Y_{H_2O,lim}(t,x)\right)\end{aligned} \tag{17}$$

$$Y_{H_2O,lim}(t,x) = \frac{1}{\rho_{exh}(t,x)v_{H_2O,lim}(t)} \tag{18}$$

$$\begin{aligned}\dot{m}_{H_2O,th}(t,x) \\ = -\frac{A_{in}h_{in}(t,x)(T_{exh}(t,x) - T_{cat}(t,x))}{\Delta H_{evap}}\end{aligned} \tag{19}$$

5) The exhaust gas temperature is updated using the heat equation:

$$\begin{aligned}\frac{\partial T_{exh}(t,x)}{\partial t} \\ = \frac{h_{in}(t,x)A_{in}\cdot(T_{cat}(x,t) - T_{exh}(x,t)}{V_{exh}.\rho_{exh}(t,x).cp_{exh}(x,t)} \\ + \frac{\lambda_{exh}(x,t)}{\rho_{exh}(x,t).cp_{exh}(x,t)}\,.\,\frac{\partial^2 T_{exh}(t,x)}{\partial x^2} \\ - u_{exh}(t,x)\cdot\frac{\partial T_{exh}(t,x)}{\partial x}\end{aligned} \tag{20}$$

6) The conversion efficiency of the 3WCC for each pollutant i is obtained by the product of a linear function of gas flow and a Wiebe law (Jaine, 2004) function of 3WCC temperature. The Wiebe law form is preferred to a more classical hyperbolic tangent function (Simon, 2018) because it allows a non-symmetric shape in the ramp part of the function. This degree of freedom permits a more flexible modelling of the conversion efficiency. The mixture is supposed stoichiometric and the influence of the air/fuel ratio is consequently neglected.

$$\begin{aligned}\eta_i(t,x) \\ = \left(1 - \exp\left(-a_{T,i}\left(\frac{T_{cat}(t,x) - T_{0,i}}{\Delta T}\right)^m\right)\right) \\ \cdot\left(a_{\dot{m},i}\dot{m}_{exh}(t) + b_{\dot{m},i}\right)\end{aligned} \tag{21}$$

7) Finally, the 3WCC temperature can be updated. Here the heat equation considers both inner and outer convections, the exothermic conversion reactions, the water phase change and the conduction.

$$
\rho_{cat}(t,x)cp_{cat}(t,x)\frac{\partial T_{cat}(t,x)}{\partial t}
$$
$$
= \dot{Q}_{conv\ in}(t,x) + \dot{Q}_{conv\ out}(t,x) + \dot{Q}_{ex}(t,x) \quad (22)
$$
$$
+ \dot{Q}_{evap}(t,x) + \dot{Q}_{cond}(t,x)
$$

$$
\dot{Q}_{conv\ in}(t,x)
$$
$$
= \frac{h_{in}(t,x).A_{in} \cdot (T_{exh}(t,x) - T_{cat}(t,x))}{V_{cat} \cdot (1-\epsilon)\frac{dx}{L}} \quad (23)
$$

$$
\dot{Q}_{conv\ out}(t,x)
$$
$$
= \frac{h_{out}(t,x).A_{out} \cdot (T_{amb}(t,x) - T_{cat}(t,x))}{V_{cat} \cdot (1-\epsilon)\frac{dx}{L}} \quad (24)
$$

$$
\dot{Q}_{ex}(t,x)
$$
$$
= \sum_{i=\{CO,HC,NOx\}} \dot{m}_i(t,x) \cdot \frac{K_{reac,i}}{V_{cat} \cdot (1-\epsilon)\frac{dx}{L}} \cdot \eta_i(t,x) \quad (25)
$$

$$
\dot{Q}_{evap}(t,x) = \frac{\dot{m}_{H_2O}(t,x)\Delta H_{evap}}{V_{cat} \cdot (1-\epsilon)\frac{dx}{L}} \quad (26)
$$

$$
\dot{Q}_{cond}(t,x) = \lambda_{cat}\frac{\partial^2 T_{cat}(t,x)}{\partial x^2} \quad (27)
$$

By lack of space, the identification procedure will not be extensively developed in this paper. The thermal inertia parameters $h_{in\ min}$, h_{ext}, ρ_{cat}, cp_{cat}, λ_{cat} and the water-phase-changing parameters $D_{H_2O\ vap}$, K_{H_2O} are identified using experimental data from engine starts followed by long inactive periods; the corresponding pattern, to be repeated twice, is illustrated in Fig. 6. The pollutant conversion parameters ϕ_{canal}, K_{reac}, a_T, T_0, m, $a_{\dot{m}}$, $b_{\dot{m}}$ are identified through a mapping of the engine behaviour, as illustrated in Fig. 7. In order to assess the accuracy of this model, it is compared to a classical 0D model similar to the methods proposed in the literature of energy and pollutants management of HEVs.
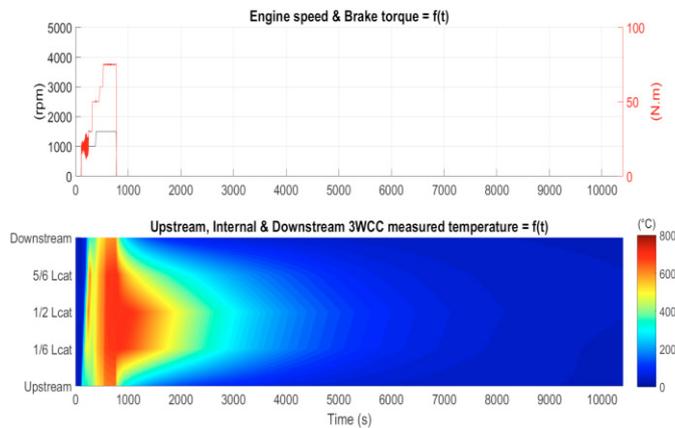

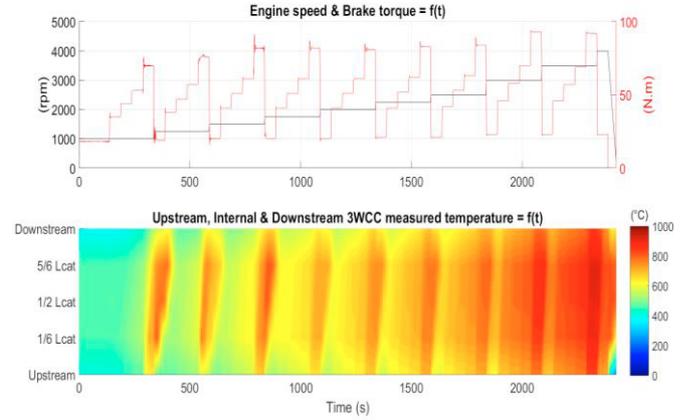Fig. 6: Experiment pattern for identification of thermal inertia and water phase changing parameters

Fig. 7: Mapping experiment for identification of pollutant conversion parameters

2.2 0D Model

The 0D model used in this paper for comparison purpose is similar to the models proposed by the vast majority of the literature of energy and pollutants management of HEVs (Eriksson, 2002; Mertz, 2012; Maamria, 2015). While the conversion efficiency is still computed using (21), the exhaust gas temperature in the 3WCC is considered equal to the upstream temperature and the water phase change effect is neglected. The 3WCC temperature is updated considering only internal and external convection and the exothermic contribution of conversion reactions:

$$
\frac{dT_{cat}(t)}{dt}
$$
$$
= (k_1 \cdot \dot{m}_{exh}(t) + k_2) \cdot (T_{cat}(t) - T_{exh}(t)) \quad (28)
$$
$$
+ k_3 \cdot (T_{cat}(t) - T_{amb}(t) + k_4 \cdot \eta_{CO}(t) \cdot \dot{m}_{CO}(t)
$$
$$
+ k_5 \cdot \eta_{HC}(t) \cdot \dot{m}_{HC}(t) + k_6 \cdot \eta_{NOx}(t) \cdot \dot{m}_{NOx}(t)
$$

The k-coefficients are all determined by identification. Whereas the 1D model presented in subsection 2.1 allows more accuracy by taking spatial gradient and water phase change into account, this 0D model is considerably simpler, thus allowing a simpler identification process and requiring modest computational resources. The estimation performances of both models are illustrated in Fig. 8, showing a warm-up phase. The 0D model does not consider spatial discretisation, hence the temperature estimated by this model is taken spatially constant in this figure. It appears that taking water evaporation into account improves largely the estimation performance; if the accuracy gain provided by the 1D model compared to the 0D model is moderate at the intake of the 3WCC, it becomes more important further in the catalyst, where water remains longer. Considering strictly the warm up phase (20s to 100s on Fig. 8), the RMSE of the spatially averaged temperature estimation is 68.53°C for the 0D model, whereas it is only 19.22°C for the 1D model. The 1D model used in this paper allows then a 72% decrease of the temperature error during warm up. Given these results, the question of the impact of this temperature estimation improvement on pollutants emissions in the context of energy and pollutants management of HEVs is investigated in the next sections.

3. OPTIMAL CONTROL STRATEGY

The reference method to solve the energy and pollutants management of HEVs problem is the Equivalent Consumption Minimization Strategy (ECMS; Paganelli, 2002), which is an application of Pontryagin Maximum Principle (Pontryagin, 1962; Serrao, 2009). More particularly, the computation of the optimal torque split is obtained using (1) and:

$$\tau_{ICE}^*(t) = \underset{\tau_{ICE}}{\mathrm{argmin}}(H(t, \tau_{ICE}(t)) \qquad (29)$$

$$
\begin{aligned}
&H\big(t, \tau_{ICE}(t)\big) \\
&= (\dot{m}_{fuel}\big(t, \tau_{ICE}(t)\big) + \alpha\, \dot{m}_{poll}\big(t, \tau_{ICE}(t)\big) \qquad (30) \\
&+ \lambda_{SOC}(t)S\dot{O}C\big(t, \tau_{ICE}(t)\big)
\end{aligned}
$$

The control value is thus obtained by minimizing at each instant a compromise between thermal and electric energy, balanced by the equivalence factor λ_{SOC}. In this paper the real-time oriented variant called Adaptive-ECMS (A-ECMS) is used, where λ_{SOC} is adapted using a PI controller to regulate the SOC around a given reference (Onori, 2011). The pollutants term $\dot{m}_{poll}$ is obtained considering the conversion efficiency provided by either the 1D or the 0D models presented earlier, as developed in section IV.

Fig. 8: Model fitting during warm-up

4. RESULTS

In order to investigate the impact of the model choice on pollutants performances, the following procedure is proposed. On one hand the A-ECMS strategy described in section 3 is used, and considers the temperature and conversion efficiency estimations of the 1D model described in subsection 2.1 (strategy denoted S1). On the other hand the same A-ECMS procedure is applied, but the temperature and conversion efficiency estimations are provided by the 0D model presented in subsection 2.2 (strategy denoted S0). In both cases the "real" temperature used in the simulation to compute the pollutants results is the temperature estimated by the 1D model, provided the good estimation performances obtained in section II. The two strategies are compared for 3 different cycles: the homologation cycle WLTP and two cycles obtained from real-driving data (respectively denoted BSG and ND, see Fig. 9). The initial 3WCC temperature is set to 20°C and the SOC reference is constant at 50%. The structure of the powertrain model is obtained from Simon (2018). Table 1 shows the performances differences obtained with S1 relatively to S0. The parameter α and the A-ECMS strategy described in section III are calibrated so that the differences between S0 and S1 in terms of respectively fuel consumption and final SOC are negligible. It appears that the strategy S1 allows a slight gain in pollutants emissions depending on the cycle: the emissions reductions are ranging from 0.93% to 2.43% for the CO, from 1.31% to 2.51% for the HC and from 0.71% to 2.78% for the NO$_x$. These improvements appear small compared to the RMSE reduction of temperature estimation (72% during the warm up phase). This phenomenon can be explained by the convergence of the temperature estimated during S0 and S1. As illustrated by Fig. 10, S0 overestimated the 3WCC temperature in the beginning of the cycle by neglecting the water presence. Overestimating the 3WCC temperature will have two consequences on its dynamic:

- The difference between the gas temperature and the estimated 3WCC temperature decreases, leading to underestimate the heat transferred to the 3WCC by internal convection,

- The difference between the ambient temperature and the estimated 3WCC temperature increases, leading to overestimate the heat lost by the 3WCC to the environment.

The temperature estimation difference between S0 and S1 comes initially from the latent heat of vaporization of the water phase change considered in S1. However, after this initial phenomenon the two mechanisms described above lead S0 to underestimate the temperature increase. Considering similar torque decisions, the temperatures estimated by S0 and S1 converge and become equal when the integral of the internal convection underestimation and external convection overestimation in S0 has fully compensated the latent heat of vaporization in S1. This phenomenon is illustrated in Fig. 10: in this real-driving cycle the convergence happened around 300°C; the temperature estimation difference between S0 and S1 existed consequently before the 3WCC could reach high efficiency conversion zones. In each cases the ECMS strategy behaved consequently in a similar, conservative manner and
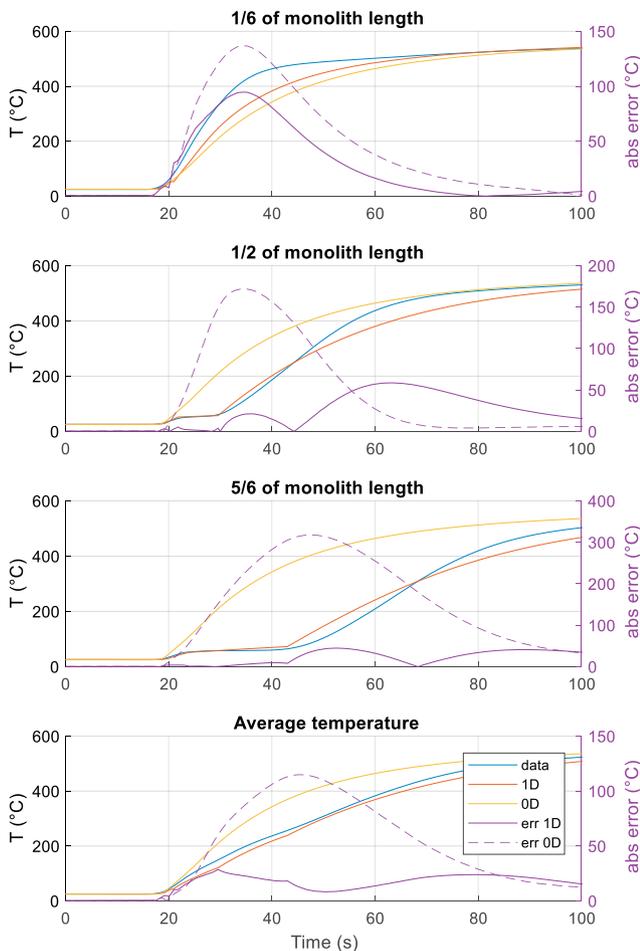
focused on pollutants during the phase preceding temperature estimation convergence. Despite an early temperature estimation difference, S0 and S1 led to close torque split decision, explaining why the emission reduction allowed by S1 appeared small compared to the temperature estimation improvement brought by its thermal model.

Table 1: S1 gains compared to S0

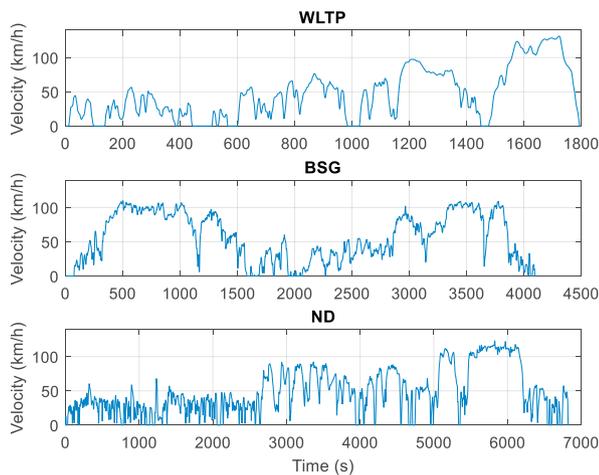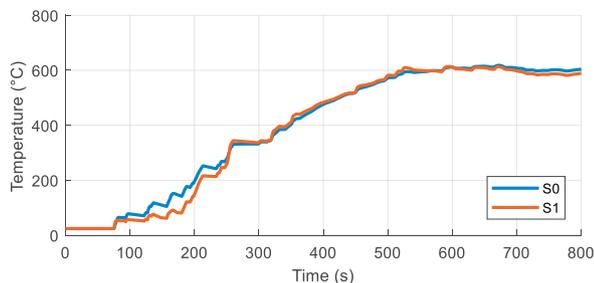| Cycle	Fuel	SOC diff.	CO	HC	NOx
WLTP	-0,02%	0,00%	2,43%	1,61%	0,71%
ND	-0,06%	0,01%	0,93%	1,31%	2,34%
BSG	-0,06%	-0,01%	1,04%	2,51%	2,78%

Fig. 9: Simulated cycles

Fig. 10: S0 overestimating the 3WCC temperature during warm up phase, BSG cycle

5. CONCLUSION AND FUTURE WORK

This paper proposes a 1D model of the 3WCC temperature, that takes into account water evaporation and condensation. Modelling water phase changing allows to increase considerably the accuracy of the temperature estimation in the warm-up phase, leading to a 72% RMSE reduction in the warm up phase, compared to a simple 0D model neglecting the liquid water presence. In the context of energy and pollutants management of HEVs, an ECMS strategy using the proposed model permitted to reduce the pollutants emissions by an order of magnitude of 1-2% compared the same strategy using the baseline model.

Future work will look in another direction by addressing the question of emissions produced during ICE transient:

- CO, HC, NOx and particulates emissions will be characterized during engine speed and torque transients (Giakoumis, 2010) and dealt with using a short-term Model Predictive Control approach,

- The impact of engine temperature on particulates generation will be investigated and an ECMS strategy considering SOC, 3WCC temperature and engine temperature will be proposed (Maamria, 2017).

REFERENCES

Aliramezani, M., Khademnahvi, M., & Delkhosh, M. (2018). Optimal energy management strategy of a hybrid electric vehicle considering engine noise. *Journal of Vibration and Control*, 24(23), 5546-5555.

Clarkson, R.J., Benjamin, S.F. (1995). Modelling the effect of moisture on catalyst warm up. *Proc. of the VTMS-2 Conference*, 555-562.

Chase, M.W. (1998). *NIST-JANAF Thermochemical Tables*. American Institute of Physics.

Di Cairano, S., Bernardini, D., Bemporad, A., & Kolmanovsky, I. V. (2013). Stochastic MPC with learning for driver-predictive vehicle control and its application to HEV energy management. *IEEE Transactions on Control Systems Technology*, 22(3), 1018-1031.

Eriksson, L. (2002). Mean value models for exhaust system temperatures. *SAE Transactions*, 753-767.

Furfaro, D., Saurel, R. (2015). Modélisation du changement de phase d'une goutte liquide entourée d'un gaz multi-constituant. *Proc. of the 22ème Congrès Français de Mécanique.*

Giakoumis, E. G., & Lioutas, S. C. (2010). Diesel-engined vehicle nitric oxide and soot emissions during the European light-duty driving cycle using a transient mapping approach. *Transportation Research Part D: Transport and Environment*, *15*(3), 134-143.

Hadj-Said, S., Colin, G., Ketfi-Cherif, A., & Chamaillard, Y. (2016). Convex optimization for energy management of parallel hybrid electric vehicles. *Proc. International Symposium on Advances in Automotive Control*, 271-276.

Jaine, T. (2004). *0D Combustion Modelling of DI Diesel engines*. Ph.D. thesis, Univ. Orléans (France).

Kuchly, J., Nelson-Gruel, D., Charlet, A., Simon, A., Jaine, T., Nouillant, C., Chamaillard, Y. (2020). Forecasting ECMS for Hybrid Electric Vehicles. *Proc. 21th IFAC World Congress.*.

Maamria, D., Chaplais, F., Petit, N., and Sciarretta, A.(2014). Numerical optimal control as a method to evaluate the benefit of thermal management in hybrid electric vehicles. *Proc. of the IFAC World Congress*,4807–4812.

Maamria, D. (2015). *Dynamic optimization in multi-states systems for automobile energy efficiency*. Ph.D. thesis, Mines ParisTech (France).

Maamria, D., Sciarretta, A., Chaplais, F., & Petit, N. (2017). Online energy management system (EMS) including engine and catalyst temperatures for a parallel HEV. *Proc. of the 20th IFAC World Congress*, 50(1), 8913-8920.

Merz, F., Sciarretta, A., Dabadie, J.C., and Serrao, L.(2012). On the optimal thermal management of hybrid-Electric

vehicles with heat recovery systems. *Oil & Gas Science and Technology*, 67(4), 601–612.

Michel, P., Charlet, A., Colin, G., Chamaillard, Y., Nouillant, C., & Bloch, G. (2012, September). Energy management of HEV to optimize fuel consumption and pollutant emissions. *In 11th International Symposium on Advanced Vehicule Control*, (p. CDROM).

Michel, P. (2015). *Energy Management of Gasoline-Electric Hybrid Vehicle equipped with Catalytic Converter by joint Fuel Consumption-Pollution Minimization. Study and Experimental Validation*. Ph.D. thesis, Univ. Orléans (France).

Michel, P., Charlet, A., Colin, G., Chamaillard, Y., Bloch, G., & Nouillant, C. (2017). Optimizing fuel consumption and pollutant emissions of gasoline-HEV with catalytic converter. *Control Engineering Practice*, 61, 198-205.

Nüesch, T., Elbert, P., Flankl, M., Onder, C., & Guzzella, L. (2014). Convex optimization for the energy management of hybrid electric vehicles considering engine start and gearshift costs. *Energies*, 7(2), 834-856.

Onori, S., & Serrao, L. (2011). On Adaptive-ECMS strategies for hybrid electric vehicles. In *Proceedings of the international scientific conference on hybrid and electric vehicles, Malmaison, France* (Vol. 67).

Paganelli, G., Delprat, S., Guerra, T.M., Rimaux, J., and Santin, J.J. (2002). Equivalent consumption minimization strategy for parallel hybrid powertrains. *Proc. 55th IEEE Vehicular Technology Conference*, 2076–2081.

Pontryagin, L.S., et al. (1962). *The mathematical theory of optimal processes*.

Sciarretta, A., di Domenico, D., Pognant-Gros, P., & Zito, G. (2014). Optimal energy management of automotive battery systems including thermal dynamics and aging. *In Optimization and optimal control in automotive systems* (pp. 219-236). Springer, Cham.

Serrao, L., Onori, S., & Rizzoni, G. (2009). ECMS as a realization of Pontryagin's minimum principle for HEV control. *Proc. American control conference* (pp. 3964-3969).

Simon, A., Michel, P., Nelson-Gruel, D., Chamaillard, Y., & Nouillant, C. (2015). Gasoline-HEV equivalent consumption and pollutant minimization strategy. *Proc. IEEE Vehicle Power and Propulsion Conference* (pp. 1-6).

Simon, A. (2018). *Energy Optimization of Gasoline and Diesel Hybrid Powertrains with Pollutants Constraints: Study and Experimental Validation*. Ph.D. thesis, Univ. Orléans (France).

Simon, A., Nelson-Gruel, D., Onori, S., Charlet, A., Jaine, T., Colin, G., Nouillant, C., Chamaillard, Y. (2019). An Observer Looks at the Temperature in the 3WCC. *Proc. International symposium on Advances in Automotive Control*, 52(5), 531-537.

Utz, T., Fleck, C., Frauhammer, J., Seiler-Thull, D., & Kugi, A. (2014). Extended Kalman filter and adaptive backstepping for mean temperature control of a three-way catalytic converter. *International Journal of Robust and Nonlinear Control*, 24(18), 3437-3453.

Appendix A: Nomenclature

Table 2: variables and parameters nomenclature

α	Compromise parameter between fuel and pollutants	w.u.
A_{cs}	Cross section area of the 3WCC	m^2
A_{in}	Inner area of the 3WCC	m^2
A_{out}	Outer area of the 3WCC	m^2
$a_{T,i}$	Wiebe parameter in the conversion efficiency	w.u.
$a_{\dot{m},i}$	Linear parameter in the conversion efficiency	s/kg
β	Weighting parameter in $\dot{m}_{poll}$	w.u.
$b_{\dot{m},i}$	Linear parameter in the conversion efficiency	w.u.
cp_{exh}	Exhaust gas heat capacity	$J/kg/K$
cp_{cat}	3WCC heat capacity	$J/kg/K$
γ	Weighting parameter in $\dot{m}_{poll}$	w.u.
$D_{H_2O\,vap}$	Water diffusion coefficient	m/s
ϵ	Volume fraction of the 3WCC occupied by the exhaust gas	w.u.
ϕ_{canal}	Hydraulic diameter of a 3WCC canal	m
H	Hamiltonian function used in the ECMS	g/s
h_{in}	Inner convection coefficient	$W/m^2/K$
h_{out}	Outer convection coefficient	$W/m^2/K$
$\Delta Hevap$	Latent heat of vaporization	J/kg
K_{mH_2O}	Mass transfer coefficient of water	m/s
$K_{reac,i}$	Exothermic coefficient for a pollutant conversion	W/kg
$k_1, \dots, k_6$	Parameters of the 0D model	Variable
κ	Weighting parameter in $\dot{m}_{poll}$	w.u.
λ_{exh}	Exhaust gas thermal conduction coefficient	$W/m/K$
λ_{cat}	3WCC thermal conduction coefficient	$W/m/K$
λ_{SOC}	Equivalence factor in the ECMS	$g/SOC\%$
L	3WCC length	m
μ_{exh}	Exhaust gas dynamic viscosity	$kg/m/s$
$\mu_{exh\,s}$	Exhaust gas dynamic viscosity at the 3WCC boundary	$kg/m/s$
m	Wiebe law parameter in the conversion efficiency formula	w.u.
$\dot{m}_{CO}$	Carbon monoxide mass flow	g/s
$\dot{m}_{HC}$	Unburnt hydrocarbon mass flow	g/s
$\dot{m}_{NOx}$	Nitrogen oxide mass flow	g/s
$\dot{m}_{poll}$	Aggregated pollutants flow	g/s

$\dot{m}_{fuel}$	Fuel consumption	g/s
$\dot{m}_{exh}$	Exhaust gas mass flow	g/s
$\dot{m}_{H_2O}$	Condensed water mass variation	g/s
$\dot{m}_{H_2O,diff}$	Water mass variation due to vapour fraction difference	g/s
$\dot{m}_{H_2O,th}$	Water mass variation due to temperature difference	g/s
Nu	Nusselt number	w.u.
η_{CO}	CO conversion efficiency	w.u.
η_{HC}	HC conversion efficiency	w.u.
η_{NOx}	NO$_x$ conversion efficiency	w.u.
P_{exh}	Exhaust gas pressure	Pa
Pr	Prandtl number	w.u.
$\dot{Q}_{cond}$	Heat flow due to conduction	W
$\dot{Q}_{conv\,in}$	Heat flow due to inner convection	W
$\dot{Q}_{conv\,out}$	Heat flow due to outer convection	W
$\dot{Q}_{evap}$	Heat flow due to water phase change	W
$\dot{Q}_{ex}$	Heat flow due to pollutants conversion	W
ρ_{exh}	Exhaust gas density	kg/m^3
ρ_{cat}	3WCC density	kg/m^3
r_{exh}	Mass ideal gas law constant for exhaust gas	$J/kg/K$
Re	Reynolds number	w.u.
$S\dot{O}C$	Battery state of charge variation	$SOC\%/s$
τ_{EM}	Electric motor torque	Nm
τ_{ICE}	Internal Combustion engine torque	Nm
τ_{ICE}^*	Optimal ICE torque	Nm
τ_{CR}	Torque request of the driver	Nm
T_{amb}	Ambiant temperature	K
T_{cat}	3WCC temperature	K
T_{exh}	Exhaust gas temperature	K
$T_{0,i}$	Wiebe parameter in the conversion efficiency	K
ΔT	Wiebe parameter in the conversion efficiency	K
u_{exh}	Exhaust gas velocity	m/s
$V_{H_2O,lim}$	Specific volume of saturated vapour at the 3WCC/exhaust gas boundary	m^3/kg
V_{cat}	3WCC volume	m^3
V_{exh}	Exhaust gas volume	m^3
$Y_{H_2O,exh}$	Water fraction in the exhaust gas	w.u.
$Y_{H_2O,lim}$	Water fraction at the 3WCC/exhaust gas boundary	w.u.